Atmos. Chem. Phys. Discuss., 12, 6263–6282, 2012
www.atmos-chem-phys-discuss.net/12/6263/2012/
doi:10.5194/acpd-12-6263-2012

Atmospheric Chemistry and Physics Discussions

Gravity wave reflection and its influence on the consistency of temperature- and wind-based momentum fluxes simulated above Typhoon Ewiniar

Y.-H. Kim[1], H.-Y. Chun[1], P. Preusse[2], M. Ern[2], and S.-Y. Kim[3]

[1]Department of Atmospheric Sciences, Yonsei University, Seoul, South Korea
[2]Institute for Energy and Climate Research – Stratosphere (IEK-7), Forschungszentrum Jülich, Jülich, Germany
[3]Next Generation Model Development Center, Seoul, South Korea

Received: 10 November 2011 – Accepted: 17 February 2012 – Published: 29 February 2012

Correspondence to: H.-Y. Chun (chunhy@yonsei.ac.kr)

Published by Copernicus Publications on behalf of the European Geosciences Union.

Abstract

For a case study of Typhoon Ewiniar performed with a mesoscale model, we compare stratospheric gravity wave (GW) momentum flux determined from temperature variances by applying GW polarization relations and by assuming upward propagating waves with GW momentum flux calculated from model winds, which is considered as a reference. The temperature-based momentum-flux profile exhibits positive biases which fluctuate with altitude and have peak values of 17–39 % at 20–40 km. We found that this deviation stems from the interference between upward and downward propagating waves. The downward propagating GWs are due mainly to partial reflections of upward propagating waves at altitudes where the background wind and stability change with height. When the upward and downward propagating waves are decomposed and their momentum fluxes are calculated separately from temperature perturbations, the fraction of the momentum flux arising from the downward propagating waves is about 4.5–8.2 %. The net momentum flux of upward and downward propagating GWs agrees well with the reference from the model wind perturbations. Global distributions of GW momentum flux can be deduced from satellite measurements of temperatures also employing GW polarization relations but using different analysis methods. The implications of this study for the GW momentum-flux observations from satellites are discussed.

1 Introduction

Gravity waves have a significant impact in the middle atmosphere by depositing their momentum and energy into the larger-scale flow (Lindzen, 1981; Matsuno, 1982; Garcia and Solomon, 1985). The amount of vertical flux of the momentum arising from gravity waves has been estimated by various measurements such as radiosonde, super-pressure balloon, research aircraft, and radar. More recently, global distribution of the gravity-wave momentum flux has been inferred from satellite observations

ACPD
12, 6263–6282, 2012

of the temperature variance. Ern et al. (2004) first estimated the momentum flux from the satellite-observed temperature variance based on the linear theory of the internal gravity waves, along with a simultaneous estimation of the vertical and horizontal wavelengths. They showed a good agreement between the global distribution of the absolute momentum flux obtained from the satellite and that from the gravity-wave parameterization by Warner and McIntyre (2001). The method of Ern et al. (2004) has been applied in various studies on gravity waves using satellite observations for both specific events and climatologies (e.g., Alexander et al., 2008; Wright et al., 2010; Ern et al., 2011).

Although possible error sources in the momentum-flux estimation using satellite-observed temperature variance are discussed in detail by Ern et al. (2004), there could be additional error sources in the momentum-flux estimation by Ern et al. (2004): first, the assumption that all observed waves propagate upward, and second, the polarization relation between the wind and temperature perturbations employed to calculate the momentum flux. The assumption has been used for the momentum-flux estimations of the satellite-observed gravity waves for other measurement methods as well (e.g., Espy et al., 2004; Hertzog et al., 2008; Li et al., 2011). However, in the middle atmosphere downward propagation of gravity waves occurs by reflection of the upward propagating waves due to the changes in the vertical wavenumber with height (e.g., Hines and Reddy, 1967; Gossard and Hooke, 1975) or from the in situ wave sources in the upper level (e.g., Holton and Alexander, 1999; Zhou et al., 2002; Chun and Kim, 2008). The downward propagating waves can modify the momentum flux significantly in both magnitude and spectral shape, as shown by Chun and Kim (2008).

In the present study, we examine the accuracy of the gravity-wave momentum-flux estimate using the temperature variance under the assumption that all the observed waves are propagating upward. For this, we used the three-dimensional mesoscale modeling result of Typhoon Ewiniar (Kim et al., 2009) that includes both temperature and wind data. First, the gravity-wave momentum flux estimated from the temperature variance using the method of Ern et al. (2004) based on the upward-propagation assumption is compared to the momentum flux that is directly calculated from the horizontal and vertical wind perturbations. Then, the polarization relations between temperature and wind perturbations are used to decompose the temperature perturbations into upward propagating and downward propagating waves. The vertical profiles of the temperature-based momentum fluxes according to the upward and downward propagating components are calculated separately, and their sum is compared with the temperature-based momentum flux considering exclusively the upward propagating waves and the momentum flux directly calculated using wind perturbations. The origin of the downward waves is also discussed. Finally, the implications of the present results for satellite measurements of the gravity-wave momentum flux are discussed.

2 Method

2.1 Data and momentum flux estimation

Data used in this study are the results of a numerical simulation of gravity waves generated by Typhoon Ewiniar (2006). The simulation was conducted by Kim et al. (2009) using the Advanced Research WRF (Weather Research and Forecasting) modeling system (Skamarock et al., 2005), and the results of the simulation were compared with the European Centre for Medium-Range Weather Forecasts (ECMWF) analysis data and the Atmospheric Infrared Sounder (AIRS) observations (Kim et al., 2009; Kim and Chun, 2010). The data set used in the present study is the three-dimensional simulation result from 01:00 UTC, 7 July to 06:00 UTC, 8 July, with a horizontal grid spacing of 27 km at 132 vertical levels from the surface to 0.1 hPa ($z = \sim 65$ km) with a vertical grid spacing of ~ 500 m in the stratosphere. The horizontal domains for the simulation and the wave analyses are illustrated in Fig. 1 of Kim and Chun (2010).

Gravity wave perturbations are obtained by subtracting the background states from the simulated variables. Here the background states are defined as 21×21 points (567×567 km) horizontal running averages of the variables. The dependency of the

Discussion Paper | Discussion Paper | Discussion Paper | Discussion Paper |

ACPD

12, 6263–6282, 2012

Gravity wave reflection

Y.-H. Kim et al.

results on the background states is discussed in Sect. 4. Hereafter, prime and overbar indicate the gravity-wave perturbation and the background state, respectively. Using the polarization relations between wind and temperature perturbations, the mean zonal-momentum flux ($F_w = \bar{\rho}\overline{u'w'}$) of upward or downward propagating gravity waves can be expressed as

$$F_T = -\frac{g^2}{2}\bar{\rho}\sum_{k,l,\omega}\frac{k}{m\bar{N}^2}\frac{|\tilde{T}|^2}{\bar{T}^2}\,, \tag{1}$$

where u, w, T, ρ, and N are the zonal and vertical winds, temperature, density, and Brunt–Väisälä frequency, respectively. The tilde indicates a complex Fourier coefficient such that $T' = \sum_{k,l,\omega}\mathrm{Re}\{\tilde{T}\exp[i(kx+ly-\omega t)]\}$, where k, l, and ω are the zonal and meridional wavenumbers and ground-based frequency, respectively. The vertical wavenumber m is obtained from the dispersion relation of the mid-frequency gravity waves, $m^2 = \bar{N}^2/\hat{c}^2$, where $\hat{c}$ is the intrinsic phase speed. Note that the sign of m is negative for upward propagating waves and positive for downward propagating waves, with the sign convention of non-negative ω. For the calculation of F_T in this study, we take the sign of m to be negative, based on the assumption that the temperature variance stems from upward propagating waves, which is often made in other studies as well (e.g., Espy et al., 2004; Boccara et al., 2008; Hertzog et al., 2008; Li et al., 2011).

2.2 Wave decomposition

Internal gravity waves can be decomposed into upward and downward propagating components, and the temperature perturbation can be written as $\tilde{T} = \tilde{T}_{\mathrm{up}} + \tilde{T}_{\mathrm{down}}$, where the subscripts up and down indicate the upward and downward propagating components, respectively. For two-dimensional (x–z) waves, horizontal winds can be obtained from the polarization relation of internal gravity waves as $\tilde{u}_{\mathrm{up}} = A\tilde{T}_{\mathrm{up}}$ and $\tilde{u}_{\mathrm{down}} = -A\tilde{T}_{\mathrm{down}}$, where $A = ig(\bar{N}\bar{T})^{-1}$ under the mid-frequency approximation and the WKB approximation. From the above equations, the Fourier coefficients of the upward

ACPD
12, 6263–6282, 2012

and downward components of the temperature perturbation are obtained as

$$\tilde{T}_{\text{up}} = (\tilde{T} + \tilde{u}/A)/2$$
$$\tilde{T}_{\text{down}} = (\tilde{T} - \tilde{u}/A)/2\,, \tag{2}$$

where $\tilde{u} = A(\tilde{T}_{\text{up}} - \tilde{T}_{\text{down}})$. This result is expanded to the three-dimensional waves by replacing $\tilde{u}$ in Eq. (2) by $(\tilde{u},\tilde{v})\cdot\boldsymbol{K}/|\boldsymbol{K}|$, where $\boldsymbol{K}$ is the horizontal wavenumber vector. Then, the momentum flux considering both the upward and downward propagating gravity waves can be obtained as

$$F_{T\,\text{total}} = F_{T\,\text{up}} + F_{T\,\text{down}} = -\frac{g^2}{2}\bar{\rho}\sum_{k,l,\omega}\frac{k}{m\bar{N}^2}\frac{|\tilde{T}_{\text{up}}|^2 - |\tilde{T}_{\text{down}}|^2}{\bar{T}^2}\,, \tag{3}$$

where the sign of m is the same as that used in Eq. (1), i.e., negative with the sign convention of non-negative ω. The difference between Eqs. (1) and (3) is that Eq. (3) uses the difference of the temperature variances from upward and downward propagating waves rather than the total temperature variances.

3 Results

Figure 1a shows profiles of the zonal momentum flux calculated directly from the wind perturbations (F_W) and estimated from the temperature variances considering only the upward propagating gravity waves (F_T). Both profiles represent a consistently decreasing trend of the momentum flux with altitude, which is due mainly to the radiative and turbulent dissipation of waves (for details, see Marks and Eckermann, 1995; Kim et al., 2005). The magnitude of F_T is, however, larger than that of F_W at most altitudes, and it fluctuates vertically. The difference between F_T and F_W is in the range of 0.25–0.34 mPa (17–39 % of F_W) at $z = 22$, 25, 28.5, 32, and 37.5 km and is 0.40 mPa (60 % of F_W) at $z = 44$ km, and the vertically averaged difference is 0.14 mPa (14 % of F_W). Figure 1b shows profiles of F_T for eastward ($\hat{c} > 0$) and westward propagating ($\hat{c} < 0$)

ACPD
12, 6263–6282, 2012

waves. The momentum flux of the westward waves is much smaller than that of the eastward waves, because most westward waves are filtered out by the stratospheric easterly winds (see Fig. 5a) in the summertime. As the momentum flux of the eastward waves is dominant and fluctuates with similar amplitudes to F_T shown in Fig. 1a, we hereafter present the results only for the eastward waves.

To clarify the origin of the vertical fluctuations in F_T, structures in the temperature variances are investigated. Figure 2a shows the x–z cross section of temperature variances for the purely eastward propagating waves (i.e., $\phi = 0$, where ϕ is the azimuthal angle of wave-propagation direction) at 00:00 UTC, 8. The variance signals are slanted eastward and reveal several nodes at fixed altitudes of 23, 26.5, 30.5, 35, and 42 km in $x > 2000$ km. Note that the altitudes of the nodes correspond to the local minima of F_T as shown in Fig. 1. These imply that waves slanted westward are superimposed with non-negligible amplitudes on the eastward slanted waves, and that the interference between the eastward and westward slanted waves is responsible for the vertical fluctuations in the profile of F_T. Given that only eastward propagating waves are considered here, a westward slant of waves indicates downward propagation.

Indeed, the vertical node structure also appears in the variance profiles of other single variables, whereas it does not appear in the zonal-mean covariance profiles. Between the variance and the covariance, two different features are found in their two-dimensional fields (Fig. 2a,b): First, the node structure is less prominent in the covariance field, and second, there are negative values of covariance between the regions of large positive covariance. The former can be explained by locations of local extremes and nodes in the fields of u' and w' (Fig. 2c,d). For the eastward slanted waves, the two variables are in phase, which result in the positive covariance. Along the phase lines, there exist local extremes and nodes in u' where the nodes and local extremes of w' are located, respectively, resulting that the covariance between u' and w' has less prominent nodes or extremes. Those two features in the covariance field (Fig. 2b) cause the differences between the zonal-mean variance and covariance profiles (and thus, F_T and F_W).

The negative values of covariance (or the negative momentum flux) for the eastward propagating waves in Fig. 2b indicates the existence of downward propagating waves. To investigate the downward propagating waves quantitatively, temperature fields are decomposed into upward and downward waves, as shown in Eq. (2), and the x–z cross sections of variances in the decomposed temperature fields are presented in Fig. 3a,b for the zonal waves at the same time as in Fig. 2a. As expected, the downward waves coexist with the upward waves in $x > 2000$ km. Both waves have similar dominant horizontal wavelengths of about 500 km, but various vertical wavelengths with height ranging from 6 to 15 km. The temperature variance of the downward waves is about 7.9 % of that of the upward waves. It is noteworthy that even though the variance of the downward waves is much smaller than that of the upward waves, effects of the interference between the two waves on the total variance fields can be significant, as shown in Fig. 2a. The x–z cross sections at other times (not shown) indicate that the ratio of the mean variance of the downward waves to upward waves is about 8.2 %, and that the altitudes of nodes are not time-dependent during 06:00 UTC, 7–00:00 UTC, 8.

The eastward propagating waves illustrated in Fig. 3 are the most abundant component for both the upward and downward waves in this simulation. For waves propagating in other directions ($\phi \neq 0$, not shown), the horizontal wavelength analysis shows broad spectra (200–660 km) with much smaller amplitudes than the zonal waves. The altitudes of nodes for these waves are relatively irregular and different from those for the zonal waves, which might result from the broad spectra of waves. Regardless of the different characteristics, the ratio of variances of the downward waves to the upward waves is about 4–8 %, which is consistent with that by the eastward propagating waves.

To quantify the difference in the momentum flux from Eqs. (1) and (3), Fig. 4 shows the profiles of the momentum fluxes for the upward and downward propagating waves as well as the sum of the two. The momentum flux of the downward propagating waves is 0.1 mPa at $z = 20$ km. This decreases at higher altitudes and oscillates with amplitudes of ~ 0.005 mPa (Fig. 4b). The ratio of the momentum fluxes of the downward

ACPD
12, 6263–6282, 2012

waves to upward waves is 4.5–8.2 %. The net momentum flux ($F_{T\,\text{total}}$) is quite close to F_W. This confirms that the errors introduced in Fig. 1 are due mostly to ignoring the interference between the upward and downward waves in the variance fields.

The good agreement between $F_{T\,\text{total}}$ and F_W also confirms that the application of polarization relations inferred from the linear gravity wave theory does not cause notable errors. The polarization relations are derived with two approximations, i.e., WKB and mid-frequency. As justified by Wright et al. (2010), the mid-frequency approximation is valid for gravity waves with horizontal and vertical wavelengths of ~ 100 and ~ 10 km, respectively. The gravity waves considered in the present study are within those wavelengths, and we found that a relaxation of the mid-frequency approximation does not change the results (not shown). In order to examine the validity of the WKB approximation, we checked whether the present gravity waves satisfy the criterion of $\delta \equiv |m_{zz}/2m^3 - 3m_z/4m^4| \ll 1$ proposed by Einaudi and Hines (1970). For a dominant wave in our case (a zonal wave with a phase speed of $10\,\text{m}\,\text{s}^{-1}$), the maximum value of δ is about 0.26, which is comfortably less than unity.

4 Discussion

The downward propagating waves identified in this case have amplitudes of 21–29 % of the upward propagating waves, based on the magnitude of their momentum flux compared with that of the upward propagating waves (4.5–8.2 %). As no apparent wave sources in the upper stratosphere are found and the characteristics of the downward propagating waves are similar to those of the upward waves, the downward propagation might be related to the reflection of the upward propagating gravity waves generated below. Figure 5 shows the background zonal winds (U), Brunt–Väisälä frequencies (N), and the corresponding squared vertical wavenumbers (m^2) obtained from the dispersion relation of a wave propagating eastward at a phase speed of $10\,\text{m}\,\text{s}^{-1}$, which was the most dominant wave revealed in Fig. 2 and Fig. 3. As the background zonal winds have negative shear in the stratosphere, m^2 of the eastward propagating wave

ACPD
12, 6263–6282, 2012

has a decreasing trend with altitude (10×10^{-7}–2×10^{-7} rad^2 m^{-2}). Note that for any waves in the mid-frequency range, m^2 is larger than zero in the present case, indicating that total reflection of waves does not take place. However, there are significant local changes in m^2 at several altitudes where N sharply decreases, which implies the existence of partial reflection of waves. For example, at $z = 27$–30.5 km, m^2 changes from 8.6×10^{-7} rad^2 m^{-2} to 4.0×10^{-7} rad^2 m^{-2}. If no reflection above $z = 30.5$ km is assumed, a simple two-layer model reveals the reflection coefficient as $|\Delta m/2\bar{m}| \approx 0.19$ below $z = 27$ km, where the numerator and denominator indicate the difference and sum of the vertical wavenumbers in the two layers, respectively (Eliassen and Palm, 1961). A more complicated model that considers the continuous changes in m^2 within $z = 27$–30.5 km using a hyperbolic tangent profile predicts the reflection coefficient as ~ 0.176 (Blumen, 1985). If there are other significant changes in m^2 and reflected downward waves above $z = 30.5$ km, the actual reflection coefficient below $z = 27$ km might be larger than the predicted value. In fact, the reflection coefficient can be the amplitude ratio of the downward waves to the upward waves in our case.

There is a possibility of wave reflection at the upper boundary of the numerical model. By using the damping layer ($z = 45$–65 km in the present case) with a depth greater than the vertical wavelength of the waves, the artificial reflection near the upper boundary can be minimized. Based on the calculations by Klemp and Lilly (1978), the expected coefficient of the artificial reflection by the damping layer is only about 0.05 or less in our case. The actual coefficient of reflection at $z = 45$ km, however, appears to be much larger (~ 0.28) than that value. There are two possibilities of obtaining the larger coefficient at the physical model top ($z = 45$ km): (i) artificial reflection at $z = 45$ km in the present simulation can be larger than that predicted in the analytical study by Klemp and Lilly (1978) based on a simple dynamic model, and (ii) the internal partial reflections might also occur above $z = 45$ km, especially near the stratopause. The relative importance of the two processes for the amount of downward propagating waves at $z = 45$ km is not clear at the moment. However, the decreasing trend and vertical oscillation of the momentum flux for the downward waves shown in Fig. 4 support

ACPD
12, 6263–6282, 2012

the notion that the wave reflection occurs internally at various altitudes by changes in the vertical wavenumber with height rather than stems artificially from the damping layer.

In this study, the vertical-mean magnitude of the bias is not so large ($\sim$ 14 %). However, the mean bias becomes much more significant when greater portions of the wave spectrum are partially reflected or some dominant waves experience total reflections, from which m^2 becomes zero under a favorable setting of the basic-state wind and stability. This may, for instance, happen in strong vertical wind gradients associated with the winter polar vortex. Total reflection of short horizontal-scale waves is likely to occur below the maximum of the polar night jet (e.g., Preusse et al., 2008), while partial reflection may occur both below and above the maximum-wind altitude (Sato et al., 2011).

In Sect. 2.1, the gravity wave perturbations are obtained by subtracting the background states that are defined as the horizontal running averages. In general, the characteristics and magnitudes of the gravity wave perturbations could be sensitive to the background states. In order to examine the dependency of the present results on the background states, we repeat the whole analyses using the background states that are obtained from the two-dimensional (x–y) 2nd-order polynomial fits. Note that for this case, the non-gravity wave components ($|\hat{\omega}| \leq |f|$ or $|\hat{\omega}| \geq N$, where $\hat{\omega}$ and f are the intrinsic frequency and the Coriolis parameter, respectively) are additionally filtered from the perturbations. The results from the two methods are generally similar, although the magnitudes of the momentum fluxes for the polynomial-fit method are $\sim$ 10 % larger (not shown), and the main conclusion of the present study is not dependent on the background states.

5 Conclusions

Based on mesoscale modeling results of Typhoon Ewiniar (Kim et al., 2009), momentum flux values inferred from temperature variances by means of the GW polarization relations are compared to a reference GW momentum flux calculated from the model winds. The momentum flux estimated from the temperatures exhibits vertical fluctuations and positive biases with peaks of 17–39 % at $z = 20$–40 km and 60 % at $z \sim 45$ km. The deviations stem from the interference between the upward and downward propagating waves, which was ignored in the original estimation by assuming all waves to propagate upward. The upward and downward waves are decomposed using the polarization relation between temperature and horizontal-wind perturbations, and the momentum flux for each wave is re-estimated. The relative magnitude of the momentum flux of the downward waves to upward waves is 4.5–8.2 %. The downward propagation of waves can be explained to a large extent by the partial reflection of the upward waves at various altitudes due to the changes in the vertical wavenumber with height, along with a minor contribution by the artificial reflection from a model dissipation layer.

In the present study, we performed the wave analysis in a horizontal direction rather than in a vertical direction, allowing us to estimate the momentum flux of each altitude independently. If the data were analyzed by a method using vertical analysis windows, the vertical fluctuations would be smoothed, but the momentum flux would still remain positively biased. In principle, this positive bias remains, unless 1) the eastward and westward slanted waves are separated by simultaneous wave analysis in horizontal and vertical directions, 2) the upward and downward waves are decomposed, for example by the method used here, or 3) covariances of two variables (e.g., u' and T') are used to estimated the momentum flux. The last two approaches require simultaneous observations of wind and temperature profiles, which is not available from satellites at present. Also the first method cannot be applied to present-day limb sounders as the horizontal sampling is too sparse, but might be applicable for future limb imaging missions. In the case discussed in this study, the fraction of downward propagating waves due to partial reflection on sharp gradients of the buoyancy frequency is rather small. Larger effects may be expected below strong wind gradients associated with the polar winter jets.

ACPD
12, 6263–6282, 2012

Acknowledgements. Part of this work was funded by ESA under the grant "Observation of Gravity Waves from Space", contract number: 22561/09/NL/AF. YHK and HYC were supported by Basic Science Research Program through the National Research Foundation of Korea (NRF) funded by the Ministry of Education, Science and Technology (20110000060).

References

Alexander, M. J., Gille, J., Cavanaugh, C., Coffey, M., Craig, C., Eden, T., Francis, G., Halvorson, C., Hannigan, J., Khosravi, R., Kinnison, D., Lee, H., Massie, S., Nardi, B., Barnett, J., Hepplewhite, C., Lambert, A., and Dean, V.: Global estimates of gravity wave momentum flux from high resolution dynamics limb sounder observations, J. Geophys. Res., 113, D15S18, doi:10.1029/2007JD008807, 2008.

Blumen, W.: Reflection of hydrostatic gravity waves in a stratified shear flow. Part I: Theory, J. Atmos. Sci., 42, 2255–2263, 1985.

Boccara, G., Hertzog, A., Vincent, R. A., and Vial, F.: Estimation of gravity wave momentum flux and phase speeds from quasi-Lagrangian stratospheric balloon flights. Part I: Theory and simulations, J. Atmos. Sci., 65, 3042–3055, 2008.

Chun, H.-Y. and Kim, Y.-H.: Secondary waves generated by breaking of convective gravity waves in the mesosphere and their influence in the wave momentum flux, J. Geophys. Res., 113, D23107, doi:10.1029/2008JD009792, 2008.

Einaudi, F. and Hines, C. O.: WKB approximation in application to acoustic–gravity waves, Can. J. Phys., 48, 1458–1471, 1970.

Eliassen, A. and Palm, E.: On the transfer of energy in stationary mountain waves, Geofys. Publik., 22, 1–23, 1961.

Ern, M., Preusse, P., Alexander, M. J., and Warner, C. D.: Absolute values of gravity wave momentum flux derived from satellite data, J. Geophys. Res., 109, D20103, doi:10.1029/2004JD004752, 2004.

Ern, M., Preusse, P., Gille, J. C., Hepplewhite, C. L., Mlynczak, M. G., Russell III, J. M., and Riese, M.: Implications for atmospheric dynamics derived from global observations of gravity wave momentum flux in stratosphere and mesosphere, J. Geophys. Res., 116, D19107, doi:10.1029/2011JD015821, 2011.

Espy, P. J., Jones, G. O. L., Swenson, G. R., Tang, J., and Taylor, M. J.: Seasonal variations

ACPD
12, 6263–6282, 2012

Title Page
Abstract | Introduction
Conclusions | References
Tables | Figures
Back | Close
Full Screen / Esc
Printer-friendly Version
Interactive Discussion

of the gravity wave momentum flux in the Antarctic mesosphere and lower thermosphere, J. Geophys. Res., 109, D23109, doi:10.1029/2003JD004446, 2004.

Garcia, R. R. and Solomon, S.: The effect of breaking gravity waves on the dynamics and chemical composition of the mesosphere and lower thermosphere, J. Geophys. Res., 90, 3850–3868, 1985.

Gossard, E. E. and Hooke, W. H.: Waves in the Atmosphere, Elsevier, Amsterdam, 1975.

Hertzog, A., Boccara, G., Vincent, R. A., Vial, F., and Cocquerez, P.: Estimation of gravity wave momentum flux and phase speeds from quasi-Lagrangian stratospheric balloon flights. Part II: Results from the Vorcore campaign in Antarctica, J. Atmos. Sci., 65, 3056–3070, 2008.

Hines, C. O. and Reddy, C. A.: On the propagation of atmospheric gravity waves through regions of wind shear, J. Geophys. Res., 72, 1015–1034, 1967.

Holton, J. R. and Alexander, M. J.: Gravity waves in the mesosphere generated by tropospheric convection, Tellus, 51A–B, 45–58, 1999.

Kim, S.-Y. and Chun, H.-Y.: Momentum flux of stratospheric gravity waves generated by Typhoon Ewiniar (2006), Asia-Pacific J. Atmos. Sci., 46, 199–208, 2010.

Kim, S.-Y., Chun, H.-Y., and Baik, J.-J.: A numerical study of gravity waves induced by convection associated with Typhoon Rusa, Geophys. Res. Lett., 32, L24816, doi:10.1029/2005GL024662, 2005.

Kim, S.-Y., Chun, H.-Y., and Wu, D. L.: A study on stratospheric gravity waves generated by Typhoon Ewiniar: numerical simulations and satellite observations, J. Geophys. Res., 114, D22104, doi:10.1029/2009JD011971, 2009.

Klemp, J. B. and Lilly, D. K.: Numerical simulation of hydrostatic mountain waves, J. Atmos. Sci., 35, 78–107, 1978.

Li, Z., Liu, A. Z., Lu, X., Swenson, G. R., and Franke, S. J.: Gravity wave characteristics from OH airglow imager over Maui, J. Geophys. Res., 116, D22115, doi:10.1029/2011JD015870, 2011.

Lindzen, R. S.: Turbulence and stress owing to gravity wave and tidal breakdown, J. Geophys. Res., 86, 9709–9714, 1981.

Marks, C. J. and Eckermann, S. D.: A three-dimensional nonhydrostatic ray-tracing model for gravity waves: formulation and preliminary results for the middle atmosphere, J. Atmos. Sci., 52, 1959–1984, 1995.

Matsuno, T.: A quasi one-dimensional model of the middle atmosphere circulation interacting with internal gravity waves, J. Meteorol. Soc. Japan, 60, 215–226, 1982.

ACPD

12, 6263–6282, 2012

Gravity wave reflection

Y.-H. Kim et al.

Preusse, P., Eckermann, S. D., and Ern, M.: Transparency of the atmosphere to short horizontal wavelength gravity waves, J. Geophys. Res., 113, D24104, doi:10.1029/2007JD009682, 2008.
Sato, K., Tateno, S., Watanabe, S., and Kawatani, Y.: Gravity wave characteristics in the Southern Hemisphere revealed by a high-resolution middle-atmosphere general circulation model, J. Atmos. Sci., doi:10.1175/JAS-D-11-0101.1, 2011, in press.
Skamarock, W. C., Klemp, J. B., Dudhia, J., Gill, D. O., Barker, D. M., Wang, W., and Power, J. G.: A description of the Advanced Research WRF Version 2, Tech. Note NCAR/TN-486+STR, Natl. Cent. for Atmos. Res., Boulder, Colo, 88 pp., 2005.
Warner, C. D. and McIntyre, M. E.: An ultrasimple spectral parameterization for nonorographic gravity waves, J. Atmos. Sci., 58, 1837–1857, 2001.
Wright, C. J., Osprey, S. M., Barnett, J. J., Gray, L. J., and Gille, J. C.: High Resolution Dynamics Limb Sounder measurements of gravity wave activity in the 2006 Arctic stratosphere, J. Geophys. Res., 115, D02105, doi:10.1029/2009JD011858, 2010.
Zhou, X., Holton, J. R., and Mullendore, G. L.: Forcing of secondary waves by breaking of gravity waves in the mesosphere, J. Geophys. Res., 107, 4058, doi:10.1029/2001JD001204, 2002.

ACPD
12, 6263–6282, 2012

Gravity wave reflection

Y.-H. Kim et al.

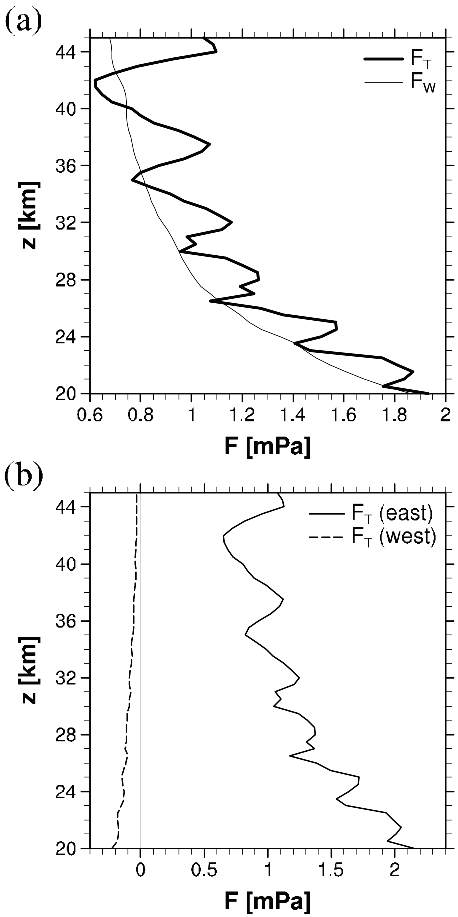

Fig. 1. Momentum-flux profiles **(a)** estimated from temperature variances (thick) and calculated from wind perturbations (thin) and **(b)** estimated from temperature variances for eastward (solid) and westward propagating (dashed) waves.

ACPD
12, 6263–6282, 2012

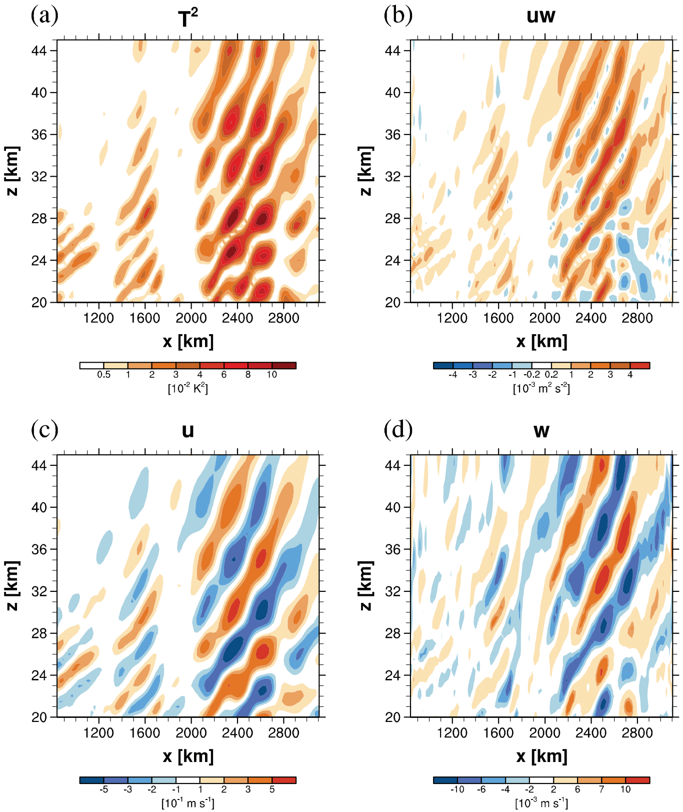

Fig. 2. *x*–*z* cross sections of **(a)** temperature variances, **(b)** covariances between the zonal and vertical wind perturbations, **(c)** zonal wind perturbation, and **(d)** vertical wind perturbation for purely eastward propagating waves (waves propagating along the *x*-axis) at 00:00 UTC, 8 July. The variables are normalized by the basic density in **(a)** and **(b)** and by the square root of the basic density in **(c)** and **(d)**.

ACPD
12, 6263–6282, 2012

Gravity wave reflection

Y.-H. Kim et al.

Title Page
Abstract | Introduction
Conclusions | References
Tables | Figures
◀ | ▶
Back | Close
Full Screen / Esc
Printer-friendly Version
Interactive Discussion

ACPD

12, 6263–6282, 2012

Gravity wave reflection

Y.-H. Kim et al.

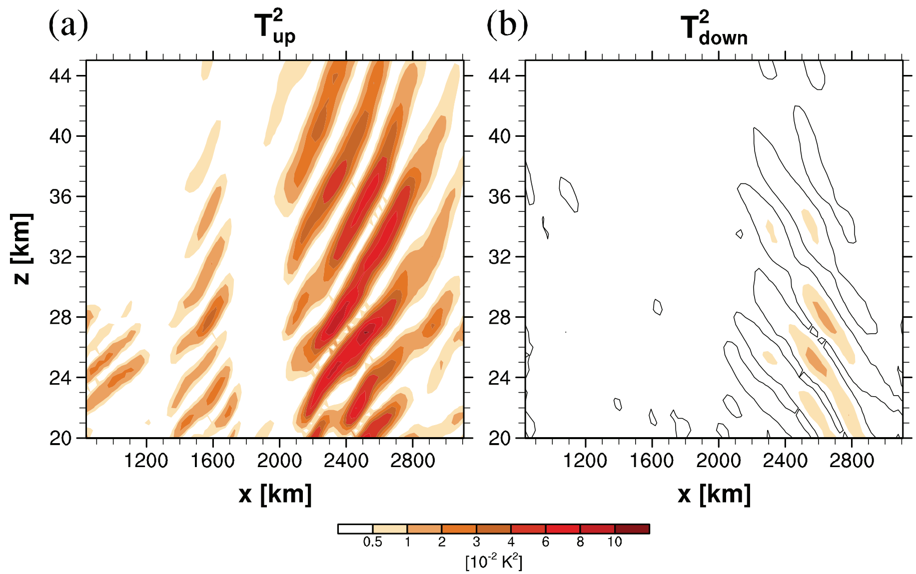

Fig. 3. The same as in Fig. 2a except for variances from decomposed components of **(a)** upward and **(b)** downward waves. In **(b)**, regions of 10^{-3} K^2 are plotted with black contours.

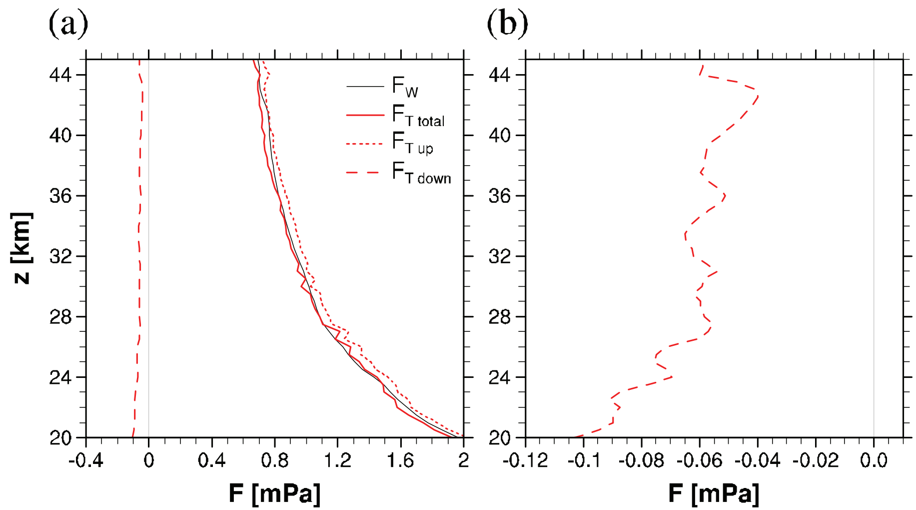

Fig. 4. **(a)** Momentum-flux profiles estimated from temperature variances by upward (red, dotted) and downward waves (red, dashed) for eastward propagating waves, and the sum of the two (red, solid). The momentum-flux profile calculated from wind perturbations for eastward propagating waves is also plotted (black, solid). The momentum-flux profile from temperature variances by downward waves is plotted again with an enlarged scale in **(b)**.

ACPD
12, 6263–6282, 2012

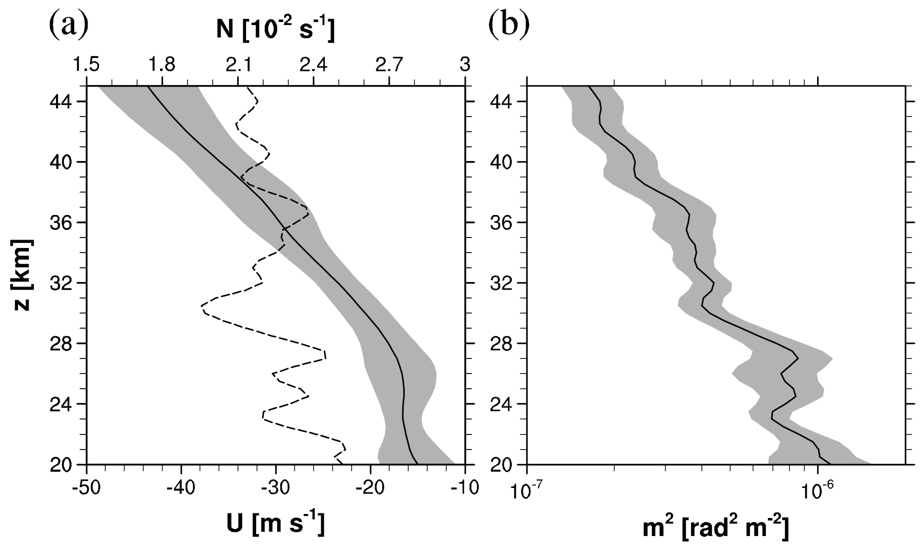

Fig. 5. Profiles of **(a)** the horizontal and temporal mean zonal wind (solid) and Brunt–Väisälä frequency (dashed) and **(b)** corresponding squared vertical wavenumber for purely eastward propagating waves at a phase speed of $10\,\mathrm{m\,s^{-1}}$ (solid). Shading indicates ranges within one standard deviation of the background zonal winds in **(a)** and of the squared vertical wavenumbers in **(b)** from their means.

ACPD
12, 6263–6282, 2012

Gravity wave reflection

Y.-H. Kim et al.